
Article:
Gupta, D., Kocot, M., Tryba, A.M. et al. (6 more authors) (2020) Novel naturally derived whey protein isolate and aragonite biocomposite hydrogels have potential for bone regeneration. Materials & Design, 188. 108408. ISSN 0261-3069

https://doi.org/10.1016/j.matdes.2019.108408

Materials and Design 188 (2020) 108408

Contents lists available at ScienceDirect

Materials and Design

journal homepage: www.elsevier.com/locate/matdes

Novel naturally derived whey protein isolate and aragonite biocomposite hydrogels have potential for bone regeneration

Dhanak Gupta [a,b,c,*], Magdalena Kocot [d], Anna Maria Tryba [d], Andrada Serafim [e], Izabela C. Stancu [e], Zbigniew Jaegermann [f], Elżbieta Pamuła [d], Gwendolen C. Reilly [a,b], Timothy E.L. Douglas [g,h]

[a] Department of Materials Science and Engineering, University of Sheffield, UK
[b] Insigneo Institute for in Silico Medicine (INSIGNEO), University of Sheffield, Sheffield, UK
[c] College of Medical and Dental Sciences, School of Dentistry, University of Birmingham, Birmingham, UK.
[d] Department Biomaterials and Composites, Faculty of Materials Science and Ceramics, AGH University of Science and Technology, Krakow, Poland
[e] Advanced Polymer Materials Group, University Politehnica of Bucharest, Romania
[f] Lukasiewicz Research Network - Institute of Ceramics and Building Materials, Ceramic and Concrete Division in Warsaw, Department of Biomaterials, Warsaw, Poland
[g] Engineering Department, Lancaster University, Lancaster, UK
[h] Materials Science Institute (MSI), Lancaster University, Lancaster, UK

HIGHLIGHTS

- Novel composite hydrogels were formed using whey protein isolate (waste product from daily industry) and synthetic aragonite via inexpensive method.
- The mechanical strength was higher for composites with higher aragonite content.
- The proliferation and alkaline phosphatase activity of seeded osteoblast-like cells was higher on composites with higher aragonite content.
- The composites degraded under physiological conditions with release of non-cytotoxic degradation products, causing mineralised extracellular matrix, suitable for bone regeneration.

GRAPHICAL ABSTRACT

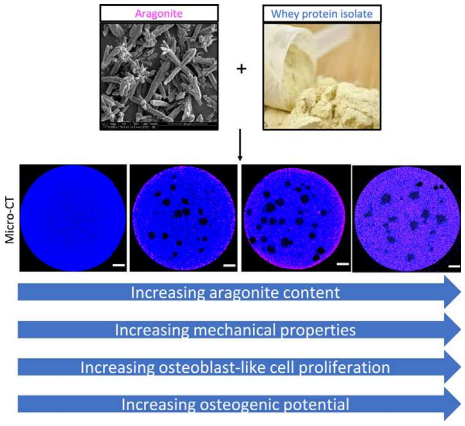

ARTICLE INFO

Article history:
Received 30 August 2019
Received in revised form 4 December 2019
Accepted 5 December 2019
Available online xxxx

Keywords:
Whey protein isolate
Aragonite
Bone graft
Inexpensive

ABSTRACT

This work explores novel biocomposite hydrogels fabricated using 40% (wt/vol) solution of whey protein isolate (WPI, from the food industry) mixed with increasing concentrations of synthetic aragonite rod-like powder of 0, 100, 200 and 300 mg/ml (named WPI0, WPI100, WPI200 and WPI300). FTIR results showed that aragonite was successfully incorporated into the WPI hydrogel network. SEM and micro-CT investigations revealed that aragonite was mainly concentrated near the edges of the composite samples, except in WPI300, which had homogeneous aragonite distribution. The pore diameters ranged from 18 to 778 μm while averaged pore size was the lowest for WPI0 at 30 μm and highest for WPI200 at 103 μm. The mean compression modulus was highest for WPI300 at 3.16 MPa. After 28 days in physiological conditions WPI300 had maximum mean swelling of 4.3% and there was the highest degradation rate for WPI200 and WPI300 and lowest for WPI100 and WPI0. The osteoblast-like MG63 cell metabolic and alkaline phosphatase activities in direct contact experiments with

* Corresponding author at: Dhanak Gupta, School of Dentistry, University of Birmingham, 5 Mill Pool Way, Edgbaston, Birmingham, B5 7EG, UK.
E-mail address: GuptaD@bham.ac.uk (D. Gupta).

https://doi.org/10.1016/j.matdes.2019.108408

Degradation
Cytocompatible

composites increased with increasing aragonite content over 3 weeks. Moreover, the degradation products of these composites were non-cytotoxic and led to mineral-like deposits in extracellular matrix. These WPI-aragonite biocomposite hydrogels are potent candidates for bone repair applications.

1. Introduction

Many orthopedic and dental complications involve the need for bone graft such as repair of traumatic and congenital defects, spinal surgery and build-up of bone stock around biomedical implants. However, the autograft or allograft bone most commonly used clinically are in limited supply [1]. Thus, synthetic biomaterials are widely explored as bone graft substitutes, these are however, not without limitations, such as release of toxic waste products, poor cellular responses by host cells and they may trigger immune responses. Bone graft substitutes can also be extremely expensive which limits their use in developing countries and even in richer developed countries [2]. Hence, there is now an increasing demand for development of inexpensive biomaterials from natural resources that can be used for bone tissue engineering and regenerative applications.

Whey protein (WP) is considered a waste product of cheese manufacturing in the dairy industry and consists of 85–90% water and 10–15% lactose, proteins, lipids and minerals. The proteins usually include β-lactoglobulin, α-lactalbumin, glycomacropeptide, immunoglobulins and bovine serum albumin, which vary in content based on the methodology used for cheese manufacturing [3,4]. WP in its various forms as reduced-lactose whey, demineralized whey, whey protein concentrates, and whey protein isolates (WPI), is used for cosmetic and pharmaceutical applications and also as emulsifying, thickening, gelling, foaming, and water- binding agents [5,6]. WP has gained widespread attention as a food additive. As WP is rich in essential amino acids such as leucine, valine, isoleucine and cysteine, the raw whey can be used for biotransformation feed, bioproteins, prebiotics and bioactive peptides after fermentation and enzymatic hydrolysis [4,6].

WPI (a type of WP) contains at least 90% protein. This is because the fat and lactose is removed via ion exchange followed by concentration and spray drying; or microfiltration followed by ultrafiltration and spray drying [7]. WPI solution can undergo gelation by heating to high temperatures, causing the unfolded proteins to form new inter-and intra-protein bonds that create a gel network. Gelation can also be achieved by high pressures, acidification or enzymatic hydrolysis [8]. Hydrogels made from WPI are widely explored as drug delivery vehicles for controlled drug release [9].

Hydrogels are three dimensional polymeric scaffolds which are hydrophilic in nature. They are explored for tissue engineering applications due to their ability to retain water, easy transport/entrapment of nutrients or cells, controlled biodegradability (useful for controlled release of bioactive components), superior mechanical strength, mouldability to desired geometry for implantation or injection (for minimally invasive procedures), excellent biocompatibility and reduced inflammatory responses [10]. For hard tissue engineering applications, hydrogels are often combined with inorganic components such as hydroxyapatite, tricalcium phosphate, bioglass particles or carbon nanotubes to increase their mechanical strength and osteoconductivity [11]. Naturally-derived hydrogels based on collagen, gelatin, alginate and chitosan have been widely reported [10], however, WPI-based composite hydrogels have only recently been reported. Dziadek et al., [12] developed novel composites where WPI was used as a main hydrogel matrix component (40% wt/vol), gelatin as a matrix modifier (20% wt/vol) and α-tricalcium phosphate (α-TCP) as inorganic component (20–70% wt/vol). They reported that increasing the α-TCP concentration linearly improved the mechanical properties of corresponding composites when compared to control hydrogels.

Aragonite is another type of inorganic phase of calcium carbonate of interest [13,14]. This is a polymorphic form of calcium carbonate naturally derived from marine coral and porous skeleton of marine corals [15]. Previously, rod-like aragonite crystals have been used to manufacture porous polymeric scaffolds based on neat poly(ε-caprolactone) for bone tissue engineering applications [16]. Moreover, a recent study showed that new bone formation was higher in the *Porites* coral and *Acropora* coral constructs than in either the β-tricalcium phosphate or banked bone constructs in ectopic, subcutaneous-pouch sheep model [17]. This suggests suitability of aragonite for bone tissue engineering and regeneration. Therefore, we report here for the first time the development of novel biocomposite hydrogels based on WPI and aragonite powder for bone tissue engineering applications.

2. Methods

2.1. Manufacturing of WPI-based biocomposites

A 40% WPI solution was obtained by adding 4 g WPI (Whey Protein Isolate, Davisco, USA) to 10 ml distilled water. After incubation in an ultrasonic bath for 20 min, 1 ml WPI solution was put into Eppendorf tubes. Synthetic aragonite rod-like powder (LUKASIEWICZ - Institute of Ceramics and Building Materials, ICiBM, Poland) as a source of $CaCO_3$ [16], was added to WPI solution in three different concentrations of 100 mg/ml (WPI100), 200 mg/ml (WPI200) and 300 mg/ml (WPI300). All samples were quickly mixed on vortex to homogenise and heated at 90 °C for 2 min to prevent sedimentation. Finally, the samples were sterilized by autoclaving in 120 °C for 2 h. WPI hydrogels without aragonite was also synthesized as a control sample (WPI0).

2.2. Scanning electron microscopy

Morpho-structural characterization of the biocomposites was performed using scanning electron microscopy (SEM). Samples were coated with a 9 nm layer of gold for 3 min at 20 mA, 0.1 mBar using Quorum Q150RES sputter coater (Quorum Technologies Ltd). SEM images were acquired using secondary electron detector JSM-7800F (JEOL UK Ltd., Welvyn Garden City) at accelerating voltage of 5 kV and a working distance of 10 mm. Biological samples were fixed in 3.7% paraformaldehyde in PBS, cleaned with sterile distilled water, dehydrated using sequential washed with 20%, 40%, 60%, 70%, 80%, 90% and 100% ethanol followed by drying by evaporation of hexamethyldisilazane, sputter coated with gold and then visualized under SEM.

2.3. Micro-CT imaging

Micro-CT scans were recorded using a SkyScan 1272 high-resolution X-Ray microtomograph (Bruker MicroCT, Belgium). The equipment uses an X-ray source with peak energies ranging from 20 to 100 kV and a 6-position automatic filter changer. The samples were scanned in sealed 2 ml polypropylene test tubes, as synthesized, to avoid dehydration. The tubes were fixed on the sample holder using modelling clay. The control sample was scanned without filter, at 45 kV and 200 μA emission current. In order to get a better contrast between the

organic and inorganic phase of the composite hydrogels, a filter of Al 0.5 mm was used. The composites were scanned at a voltage of 70 kV and an emission current of 140 μA. At least 1100 slices were registered for each sample with a rotation step of 0.2 and an averaging of 3 frames. The images were registered at a resolution of 2452 × 2452 and a pixel size of 9.5 μm for the control samples and 9 μm for the composite samples. All images were processed using Image J version: 2.0.0-rc-69/1.52p. 3D tomographies were generated using 3D viewer. The raw images were thresholded between 0 and 129 for WPI signal and 129–255 for aragonite to identify the distribution of aragonite within the samples. To investigate any fabrication architecture heterogeneity, porosity, pore size and strut size (material thickness between pores) measurements were performed for raw images (without separating WPI and aragonite) using BoneJ2 plugin in Image J [18].

2.4. Fourier transform infrared spectroscopy

The structure of the samples was examined using Fourier Transform Infrared (FTIR) Spectroscopy (Agilent Technology, UK). The spectra were collected between 4500 and 500 cm^{-1} spectral range with a resolution of 4 cm^{-1} and an average of 8 scans.

2.5. Compressive strength

The compression modulus of the wet biocomposites was determined by using a universal testing machine (Inspekt mini; Hegewald & Peschke Meß- und Prüftechnik GmbH, Nossen, Germany). Displacement rate was set to 2 $mm \cdot min^{-1}$ until failure of the samples was reached. The applied force was measured with a 100 N load cell. The compressive stress σ was then determined from the formula:

$$\sigma = \frac{F}{A}$$

where, F = applied force and A = cross-sectional area (diameter was assumed to be the same as the internal diameter of the Eppendorf tube). The compression modulus was determined by the gradient of the linear-elastic range of the stress-strain curve for small strains.

2.6. Swelling analysis

Autoclaved samples were incubated in simulated body fluid (SBF). After 1, 4, 7, 14, 21 and 28 days of incubation, samples were dried on absorbent paper to remove unbound water from the surface and then weighted. The swelling ratio of each sample was calculated as:

$$\frac{\text{weight after swelling} - \text{weight before swelling}}{\text{weight before swelling}} * 100$$

2.7. Bicinchoninic acid assay

The samples were incubated in phosphate-buffered saline (PBS, Gibco) at 37 °C and the amount of protein released into solution was measured after 1, 4, 7, 21 and 28 days of incubation. The released protein was calorimetrically detected and quantified using bicinchoninic acid (BCA) assay (Pierce BCA Protein Assay Kit, Thermo Fisher Scientific). Briefly, 25 μl of each solution was put into two wells of 96 well plates and topped up with 200 μl of BCA working reagent, which was prepared by mixing 19 ml reagent A and 0.38 ml reagent B until it was a uniform light green colour. Protein assay containers were sealed and incubated at 60 °C for 15 min. Absorbance was measured at 562 nm using a Tecan Infinite 200 Pro (Tecan, UK). Protein content was extrapolated using a standard curve from eight serial dilutions of 5 mg/ml solution of WPI in water.

2.8. Preparation of WPI-based composites for cell culture

Autoclaved samples were washed with PBS three times, followed by two culture medium washes (see Section 2.9 for culture medium composition) and then left in culture medium for 30 min before seeding cells for direct-contact cytocompatibility experiments or adding culture medium only for indirect-contact cytocompatibility experiments.

2.9. Culturing of MG63 cells

The MG63 osteoblast-like cells (passage 15 to 28) were maintained in standard culture medium composed of α-MEM Eagle with sodium bicarbonate (Sigma-Aldrich, UK), 10% Foetal Bovine Serum (LabTech, UK), 2 mM L-Glutamine and 100 mg/ml Penicillin–Streptomycin at 37 °C and 5% CO_2. At 90% confluence, cells were trypsinised, collected and seeded at 30,000 cells/sample/500 μl on composites for direct contact experiments or 30,000 cells/well/500 μl in 48-well plates for indirect contact experiments. The next day, in the case direct-contact cytocompatibility experiments, medium change was performed and then subsequently every 2–3 days of culture until Day 21. Cell metabolic activity (-Section 2.11) measurements were taken on Day 1, 4, 7, 14 and 21 of culture.

2.10. Indirect-contact cytocompatibility assessment

Effect of degradation products of composites on MG63 cells was evaluated using indirect contact cytocompatibility experiments, wherein composites were prepared for cell culture (Section 2.8) and 500 μl of culture medium per sample was added. Same day, cells were also seeded as described in Section 2.9 in 48-well plates. The next day, the eluted culture medium from samples was removed and replaced with fresh culture medium. The removed medium was added onto the cells seeded a day before in well plates. This was repeated for the next 6 days. On Day 1, 4 and 7 of culture in eluted medium, cell metabolic activity was assessed as described in next section.

2.11. Cell metabolic activity assay

Cell metabolic activity was measured using Resazurin Reduction assay. The Resazurin Stock solution of 1 mM was prepared in deionised water and for working solution, the stock was diluted 1 in 10 with prewarmed Hanks Balanced Salt Solution. At selected time points, culture medium was removed and cells were washed with PBS before adding Resazurin working solution and incubating at 37 °C and 5% CO_2. Resazurin working solution was also added to three wells or composites containing no cells (blanks). During the kinetic phase of reaction, 100 μl aliquots per well were taken and the fluorescence intensity was measured using 530 nm excitation and 590 nm emission filters on an Infinite F200 PRO microplate reader (Tecan, UK). Cell metabolic activity was expressed after subtracting the reading for unreduced (blank) reagents, normalising to reaction time and then normalising to Day 1 measurements of 0 mg/ml aragonite containing WPI gels for direct-contact cytocompatibility experiments or to Day 1 measurements of control (medium with no hydrogel composites) for indirect-contact cytocompatibility experiments. Results from two independent experiments were combined and shown.

2.12. Giemsa stain

Giemsa's solution is a mixture of methylene blue, eosin, and Azure B and stains the nucleus dark blue and cytoplasm blue to pink. Culture medium was removed, samples were fixed with 3.7% PFA in PBS for 10 min, then washed with deionised water to remove any residual fixative before immersing them in Giemsa stain for 30 min at room temperature (RT). Samples were then washed with deionised water to remove any residual stain and were ready to be imaged.

2.13. Alkaline phosphatase activity and DNA assays

On Day 21 of direct-contact cytocompatibility experiments, the culture medium was removed and the cells were washed with PBS before adding sterile deionised water (same volume as culture medium). Samples were lysed through three cycles of freeze thawing at −80 °C. Alkaline phosphatase (ALP) activity was measured using *p*-Nitrophenyl Phosphate (PNPP) Phosphatase Substrate (Thermo Scientific, UK). Briefly, 100 μl of cell lysates (or sterile distilled water for 3 blank wells to remove background) and 100 μl of substrate was added to each assay well and absorbance at 405 nm was measured on an Infinite F200 PRO microplate reader for 80 min. For DNA assay, cell lysates were diluted 1 in 10 by adding 10 μl lysates to 90 μl buffer provided by the kit. The test lysates were loaded on to a flat transparent 96-well plate (Grenier) and DNA content was quantified using Quant-i™ PicoGreen® dsDNA Assay kit (Thermofisher Scientific, UK) according to manufacturer's instruction. Briefly, 100 μl of PicoGreen working solution (1 in 200 dilution of dye with Tris-EDTA buffer) was added to each test well and three blank wells containing only water. After 10 min incubation period at RT, florescence intensity readings were taken on an Infinite F200 PRO microplate reader using 480 nm excitation and 520 nm emission filters. The DNA concentration was extrapolated using a standard curve prepared from standard DNA calf thymus provided with the assay kit. ALP activity was expressed after normalising to respective DNA contents of the samples and then to Day 1 measurements of 0 mg/ml aragonite containing WPI hydrogels.

2.14. Alizarin red S staining

Alizarin red S staining was performed to assess amount of calcium in the extracellular matrix. Culture medium was removed and cells were washed once with PBS at RT for 5 min, before fixing

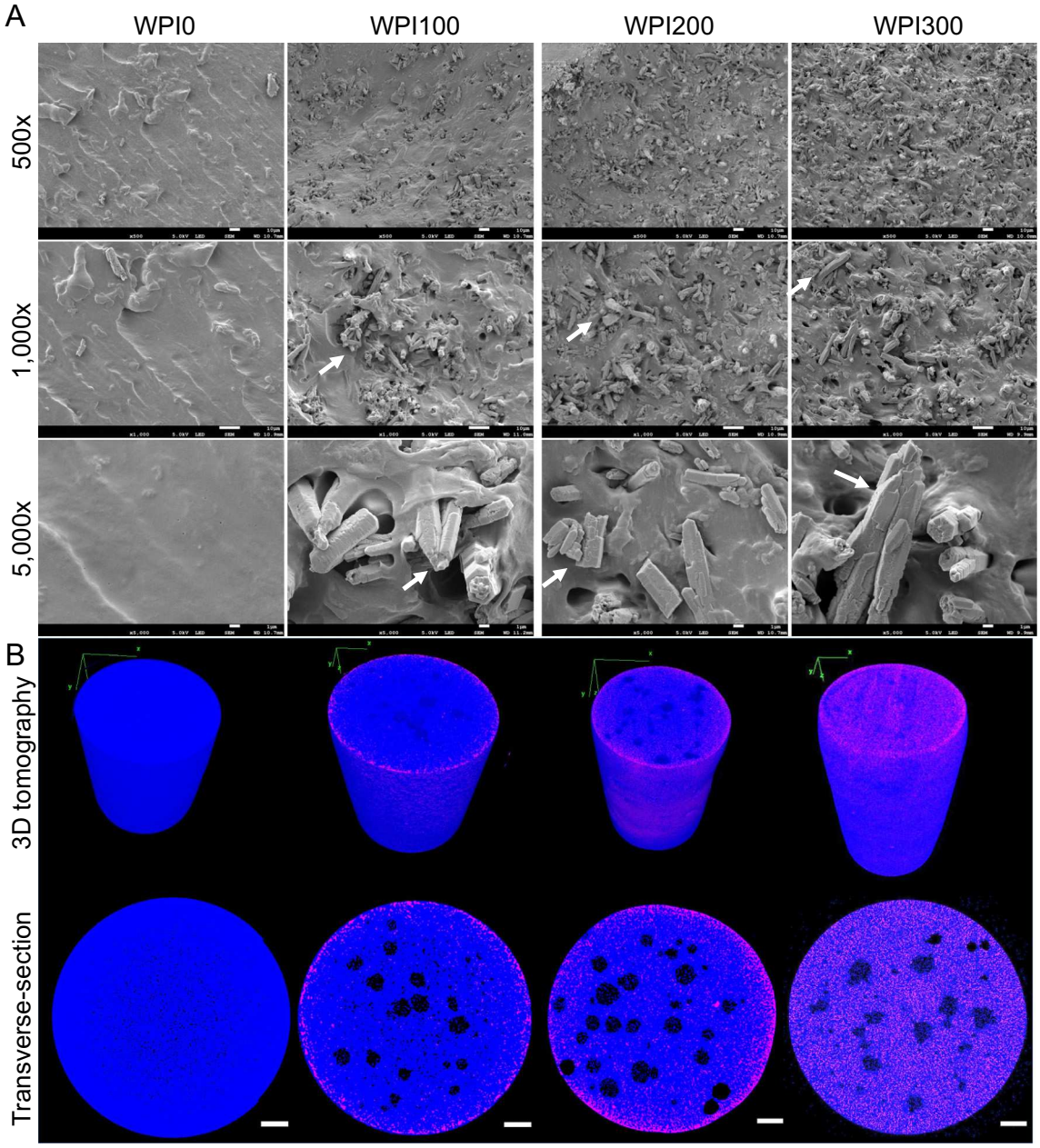

Fig. 1. Morphological analysis of WPI-based biocomposites. (A) Scanning electron micrographs of transverse-sections were acquired at three magnifications of 500×, 1000× and 5000× with scale bars of 10 μm, 10 μm and 1 μm, respectively. (B) 3D tomography and cross-sectional view of each composite is shown. Blue- WPI gel and and pink - aragonite. Scale bar = 1 mm. (For interpretation of the references to colour in this figure legend, the reader is referred to the web version of this article.)

them with 3.7% paraformaldehyde in PBS for 10 min. After removing the fixative, cells were again washed with PBS and then stained with 1% (wt/vol) solution of Alizarin red S for 30 min at RT. Then staining solution was removed and cells were washed with deionised water to remove any unbound stain. At this stage images of cells were taken.

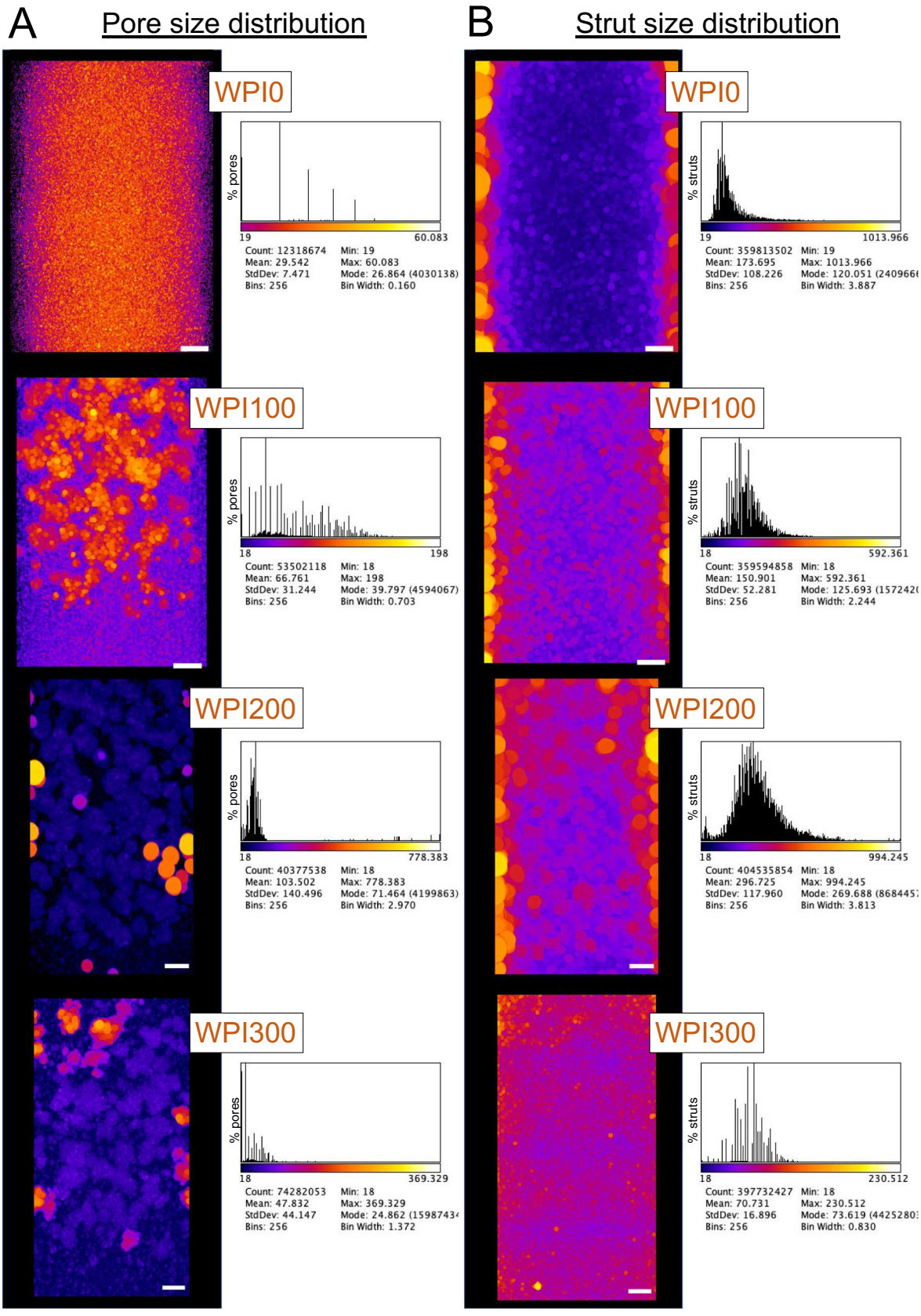

Fig. 2. Heat maps and histograms (in μm) of (A) pore and (B) strut size distributions in different WPI-based biocomposites. Scale bars = 1 mm.

2.15. Statistical analysis

All statistical analyses were performed using GraphPad Prism version 7.0d. Two experiments for every assessment were performed. Mean and standard deviation were computed for at least 6 replicates in all experiments. For comparisons one-way or two-way ANOVA was performed. WPI gel type and Day were two fixed factors. For pairwise comparisons, post-hoc analyses using Least Significant Difference, equivalent to no adjustments, were carried out. *P* values < .05 were considered significant. *, ** and *** indicate $p < .05$, $p < .005$ and $p < .0005$, respectively.

3. Results

3.1. Morpho-structural characterization of WPI-based biocomposites

SEM images showed that all the biocomposites present a typical biphasic microstructure, consisting in aragonite microrods dispersed into the WPI continuous matrix (Fig. 1A), while the control sample WPI0 has a typical appearance for amorphous polymers. It can be noticed that a smaller number of aragonite micro-rods are embedded into the WPI100 polymer matrix, while increasing the amount of mineral from WPI100 to WPI300 generated a more homogeneous distribution of the aragonite crystals in the biocomposites.

Additionally, aragonite agglomerates appeared to have different dimensions in all the investigated scaffolds. The microstructure of these particles was investigated before autoclaving (Supplemental Fig. 1). They also exhibited rod-like morphology, having various sizes. No obvious difference in morphology was observed between the particles before autoclaving and the particles in autoclaved composite samples.

To study the internal architecture of composites, micro-CT analysis was also performed. The results (Fig. 1B) indicated that at smaller aragonite content, the mineral concentrated mostly near the edges of cylindrical WPI100 and WPI200 samples, while it was more homogenously dispersed in the composite with the highest mineral content, WPI300. As expected, the control sample, WPI0, was monophasic, corresponding to the polymer matrix. Using image analysis, a volumetric porosity of 3.3%, 12.9%, 9.1% and 15.7% was calculated for WPI0, WPI100, WPI200 and WPI300, respectively.

Further image analysis revealed variable distribution of pores and struts across all composites (Fig. 2). Overall, the largest pores up to 778 μm and 369 μm were present in WPI200 and WPI300, respectively; while the largest struts of 1014 μm and 994 μm were present in WPI0 and WPI200, respectively. For all samples, the majority of pores

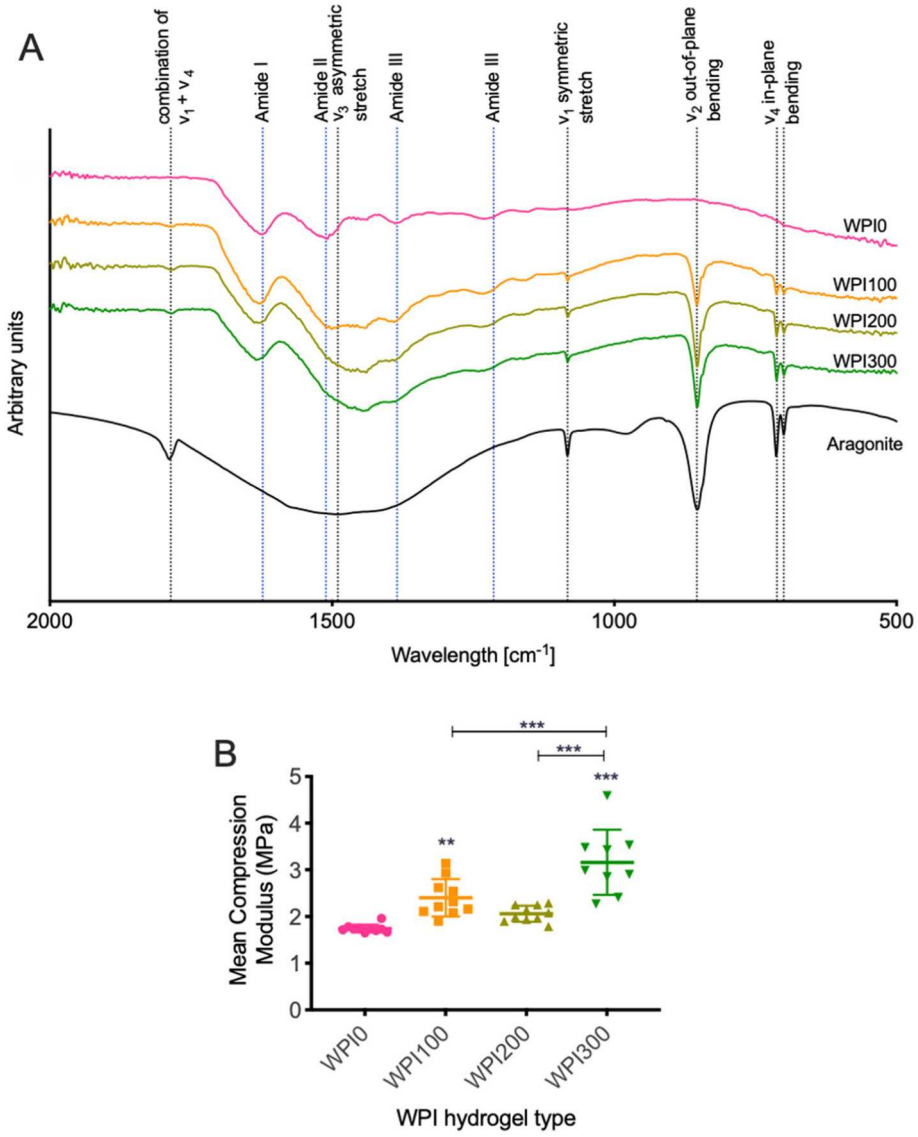

Fig. 3. (A) FTIR spectra and (B) compression modulus measurements of WPI-based biocomposites. ** and *** indicate $p < .005$ and $p < .0005$, relative to WPI0, unless otherwise mentioned.

were < 200 μm in diameter, however struts were much larger with a mean width of 297 μm in the case of WPI200, compared to all other samples. For WPI0, WPI100 and WPI300, there seemed to be larger struts near the edges and smaller struts in the centre of the composites. On the other hand, in WPI300 there appeared to be several layers of larger and smaller struts from top to bottom. In WPI100, the pore density reduced from top to bottom of the sample, which was not the case in WPI200 and WPI300. In WPI0, there were larger pores in the centre of the composite compared to its circumferential edges.

3.2. FTIR analysis

The chemical composition of biocomposites was assessed through FTIR analysis as it helps identify organic and inorganic compounds (Fig. 3A). Pure aragonite showed typical peaks for CO_3^{2-}: ν_1 - symmetric stretching at ~1083 cm^{-1}, ν_2 - out-of-plane bending modes at ~854 cm^{-1}, ν_3 - a very broad doubly degenerate planar asymmetric stretching at ~1490 cm^{-1} and ν_4 - doubly degenerate in-plane bending at ~700 cm^{-1} and ~712 cm^{-1}. There is also a peak at ~1786 cm^{-1} due to combination of the vibration frequencies assigned between ν_1 and ν_4 [19,20]. These peaks were also visible for WPI100, WPI200 and WPI300 and as the concentration of aragonite increased in hydrogels, the peak intensities also increased. As expected, these peaks were not present in WPI0, instead WPI0 exhibited typical amide I peak at ~1623 cm^{-1} from C═O stretching, amide II peak at ~1511 cm^{-1} from N—H bending coupled with C—N stretching and amide III peaks at ~1385 cm^{-1} and ~1214 cm^{-1} from C—N stretching and N—H bending [21]. It was interesting to note that as the aragonite content increased, the amide III peak at ~1385 cm^{-1} diminished and ν_3 peak was more prominent. This illustrated that hydrogels were chemically modified after aragonite addition.

3.3. Mechanical properties of biocomposites

Generally, composites containing aragonite had higher compression modulus than control samples (Fig. 3B). There was no clear correlation between resistance to compressive loading and aragonite concentration. However, the highest compression modulus was observed for WPI300 (3.16 ± 0.70 MPa). These results indicated that incorporation of aragonite particles in WPI-based composites had a reinforcing effect on the mechanical strength of composites.

3.4. Swelling analysis of biocomposites

Swelling behaviour of the studied composites is presented in Fig. 4A. After 1 day of incubation in SBF all samples swelled and the swelling ratio increased with increasing amount of aragonite from 2.5 ± 1.1% for WPI0 to 6.9 ± 2.9% for WPI300. This trend was apparent on all subsequent time points with statistically significant differences observed on Days 4, 7, 14 and 21. Additionally, all samples swelled between Day 1 to Day 4, except WPI100, for which the swelling ratio did not change until Day 28, amounting to 1.3 ± 1.6%. In the case of WPI100, the swelling ratio decreased from Day 4 to Day 28, measuring 2.2 ± 2.7%. Finally, the swelling ratio of WPI200 and WPI300 did not change between Day 4 to Day 21, it dropped to 1.8 ± 0.6% and 4.3 ± 2.8%, respectively on Day 28.

3.5. Degradation of biocomposites

Degradation of composites in PBS was measured over 28 days using BCA assay (Fig. 4B). All composites exhibited similar degradation behaviour until Day 7, where the release of protein was <1.0 mg/ml. However, significant differences were observed on Days 14, 21 and 28 of incubation in PBS. The highest degradation rate was for WPI200 and WPI300, followed by WPI100 and slowest in the case of WPI0. At the end of 28 days protein content measured 3.5 ± 0.2, 3.3 ± 0.4, 2.7 ± 0.3 and 2.0 ± 0.4 mg/ml, respectively.

3.6. Cell attachment and growth on biocomposites

To assess osteoblastic MG63 cell attachment and growth cells were seeded on composites and cell metabolic activity was measured from Day 1 to Day 21 of culture (Fig. 5A). There were no significant differences between conditions on Day 1 and Day 4 of culture. However, when cell metabolic activity was measured on subsequent time points there was higher cell metabolic activity with increasing aragonite content on Days 7, 14 and 21 of culture indicating the cell numbers increased on these scaffolds suggestive of proliferation. SEM imaging was performed on Day 7, where the cells showed a rounded morphology in dehydrated samples of all conditions except WPI300 (Supplementary Fig. 2); and Giemsa staining was performed on hydrated samples from Day 21, which confirmed that as the aragonite content increased in WPI hydrogels, the cell numbers also increased.

3.7. Alkaline phosphatase activity of cells on biocomposites

ALP activity of MG63 cells was measured after 21 days of culture on composites and the results in Fig. 5C showed nearly 10 times higher mean ALP activity of cells grown on WPI300 compared to all other conditions. These results strongly suggested that aragonite in WPI300 may have supported the cells to mature as ALP is upregulated prior to bone cell mineralisation.

3.8. Effect of degradation products of biocomposites

To investigate if cells were affected by degradation products of WPI-based composites, cells were grown in medium containing composite eluate. On days 1 and 4 of culture, there were no statistically significant differences between any of the conditions (Fig. 6A). On the Day 7, there was slightly higher cell metabolic activity in medium eluate from WPI0 or WPI200 gels relative to control.

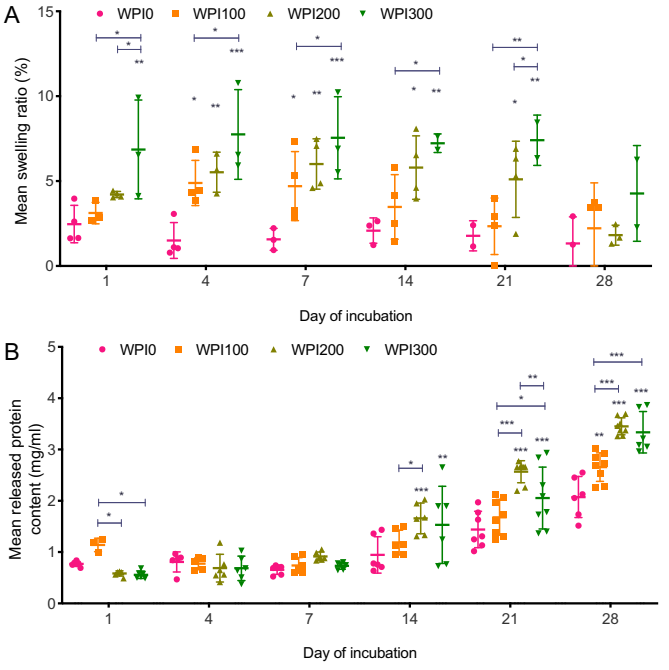

Fig. 4. Mean ± S.D. of (A) swelling and (B) protein release (degradation) analyses of WPI-based composites over 28 days in SBF and PBS, respectively.*, ** and *** indicate $p < .05$, $p < .005$ and $p < .0005$, respectively relative to WPI0 on same time point, unless otherwise mentioned.

To further assess the matrix formation by cells under the influence of the degradation products of biocomposites, cells were grown in eluted media for 21 days and then stained with Alizarin red S on Day 21 of culture. The cells grown in control (medium only) and WPI0-conditioned medium had no mineral-like deposits (Fig. 6B). However, for cells grown in medium eluted with WPI100, WPI200 or WPI300, there were several mineral-like deposits visible, with highest in the case of WPI300 that stained positively for Alizarin red S.

4. Discussion

This study established that novel WPI-aragonite biocomposite hydrogels can be manufactured via an inexpensive method. Moreover, these biocomposites are mechanically stable, undergo swelling, degradation and are also cytocompatible with osteogenic potential.

Recently, Dziadek et al. [12] reported inhomogeneous distribution of α-TCP particles and presence of porosity in WPI/gelatin/α-TCP composite hydrogels, irrespective of α-TCP concentration used. They showed more pores at the top compared to the bottom of the composites. Such an architecture of composites was attributed to rapid dissolution of calcium ions from α-TCP in the WPI/gelatin solution that may have caused the WPI around α-TCP to form aggregates, thus hindering their uniform distribution in the solution. In this study, the addition of aragonite at 100 mg/ml and 200 mg/ml to a WPI solution also lead to inhomogeneous distribution of aragonite inside the composites. However, this was not seen in the case of WPI300 (40% wt/vol WPI gel containing 300 mg/ml of aragonite). The composites had a porous architecture and the porosity increased almost 3–5 times after incorporation of aragonite. Porosity decreased with increasing distance from the top of the WPI100 composite but this was not observed for WPI200 and WPI300, where pores seemed to more evenly distributed. At the same time, bigger strut sizes were clearly visible in the circumferential edges of WPI0, WPI100 and WPI200 but not WPI300, where the strut distribution was again more even.

Such variation in the composites structure in the present study may be attributed to uneven gelation process of the WPI solution. The solution near the edges may have heated up faster than the internal regions causing delayed gelation of the internal regions and hence, more pores in that area. Moreover, as the aragonite content increased in the WPI solution, more calcium ions may have been released that affected gelation process differently in different composites. In WPI100 and WPI200 aragonite was mostly concentrated near the edges of the composites, therefore, these area would have undergone gelation even faster than in WPI0, causing the generation of even bigger pores in the internal regions of WPI100 and WPI200 compared to WPI0. In the case of WPI300, as aragonite was more evenly spread across the WPI solution, this may

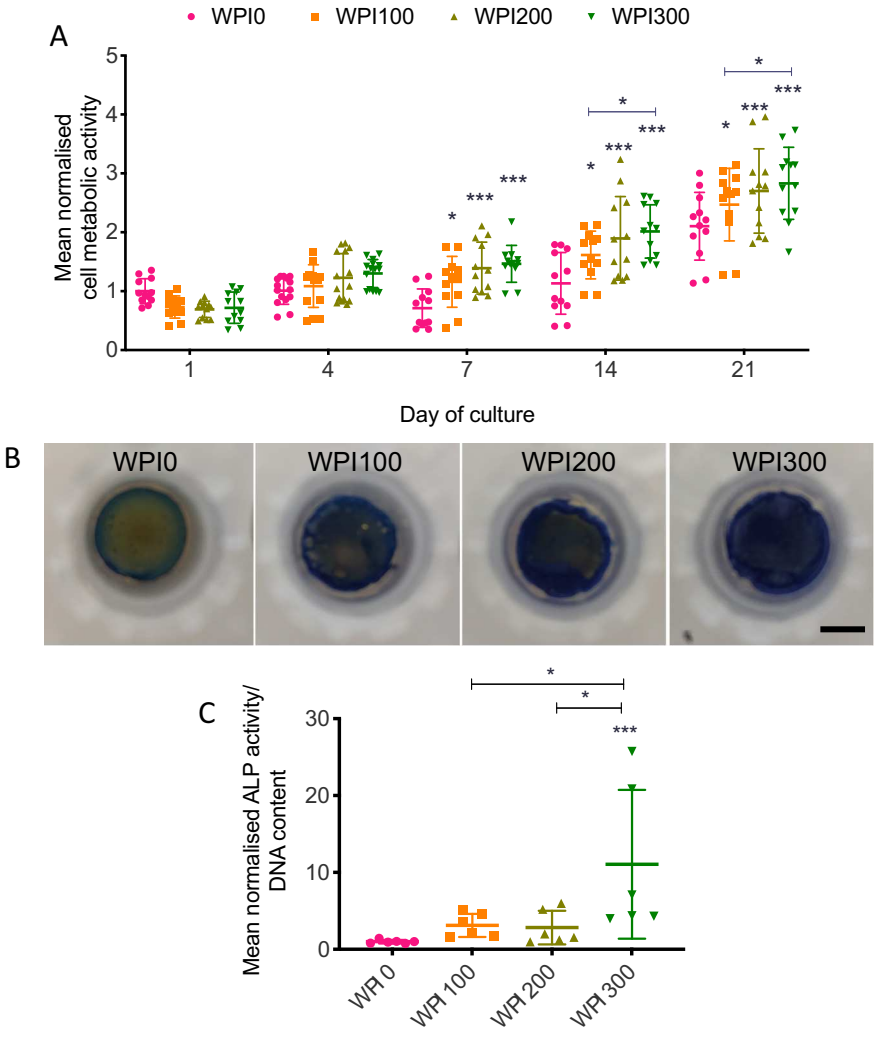

Fig. 5. Assessment of MG63 cytocompatibility with WPI-based biocomposites via direct-contact experiments. (A) Mean ± S.D. of cell metabolic activity over 21 days of culture ($n \geq 12$). (C) Composites stained with Giemsa on Day 21 are shown. Notice the increase in blue stain (cells) with increasing aragonite concentration. Scale bar = 5 mm. (C) ALP activity of cells on Day 21 on composites ($n = 6$). *, ** and *** indicate $p < .05$, $p < .005$ and $p < .0005$ relative to WPI0, unless otherwise mentioned. (For interpretation of the references to colour in this figure legend, the reader is referred to the web version of this article.)

have resulted in more homogeneous release of calcium ions across the solution, enabling a more homogeneous gelation process and pore distribution. However, this remains speculative in the absence of further data. In future, other gelation methodologies such as using infrared assisted microwave heating or high pressures [8] and higher concentrations of aragonite in WPI hydrogels may be investigated to obtain more homogeneous porosity and aragonite distribution in composites. The use of high pressure to induce gelation of dairy products is standard practice in the food industry [22].

It was expected that with linear increase in aragonite content, the mechanical strength of the composites would also increase in a similar fashion. However, no such linearity was observed but WPI300 had the highest compression modulus measured. This may again be due to the uneven distribution of aragonite and pores in WPI100 and WPI200. Interestingly, however, there was a clear positive correlation between aragonite content and MG63 cell metabolic activity and also between aragonite content and ALP activity of cells grown directly on composites, which strongly suggested that addition of aragonite was beneficial for cell proliferation and osteogenic onset.

Several studies have also shown that WP/WPI enhances proliferation of several cell types such as enteroendocrine cells [23], MC3T3-E1 osteoblastic cells [24], foetal rat calvariae osteoblasts [25], osteoblast-like Saos-2 cell, human neonatal dermal fibroblast [26] and immortalized human foetal osteoblast [27] when supplemented in culture medium. It is suggested that this effect is due to presence of β-lactoglobulin in WP/WPI, which has recently been shown to influence immunity and proliferation via receptor-mediated membrane IgM receptor in murine hybridoma cells [28]. In the present study, there was increased protein content released by composites as the aragonite content in them increased over a period of 28 days of degradation, which suggests that β-lactoglobulin from these composites may also have affected proliferation of cells grown on these composites.

WPI0 had a maximum pore size of 60 μm but after addition of aragonite in WPI100, WPI200 and WPI300 it was measured at 198, 778 and 369 μm, respectively. These pore sizes are within the recommended pore size distribution of >100 μm width for 3D scaffolds suitable for bone regeneration in vivo as smaller pores limit cell penetration and vascularisation, though they are useful for nutrient and oxygen supply and removal of waste products [29,30]. As the composites swelled more when the aragonite content increased by the end of 21 days of incubation, this may have allowed retention of more nutrients and easier removal of wastes in WPI300 compared to other composites, enabling cell growth.

Osteoblasts are able to sense local calcium concentration gradients created by osteoclast activity in bone and calcium is known to regulate differentiation of osteoblast differentiation and mineralisation process [31,32]. Higher calcium concentration can lead to osteogenic differentiation but toxic doses may lead to stress induced apoptosis-like cell death [33]. Our study showed that degradation products of WPI-based biocomposites were non-toxic and did not affect cell growth. Moreover, WPI300 had signs of intense mineralisation in the extracellular matrix by the end of 21 days of culture, maybe due to deposition of calcium salts by the cells [34,35], and/or due to degraded aragonite particles which may have directly precipitated onto the matrix. Altogether, our

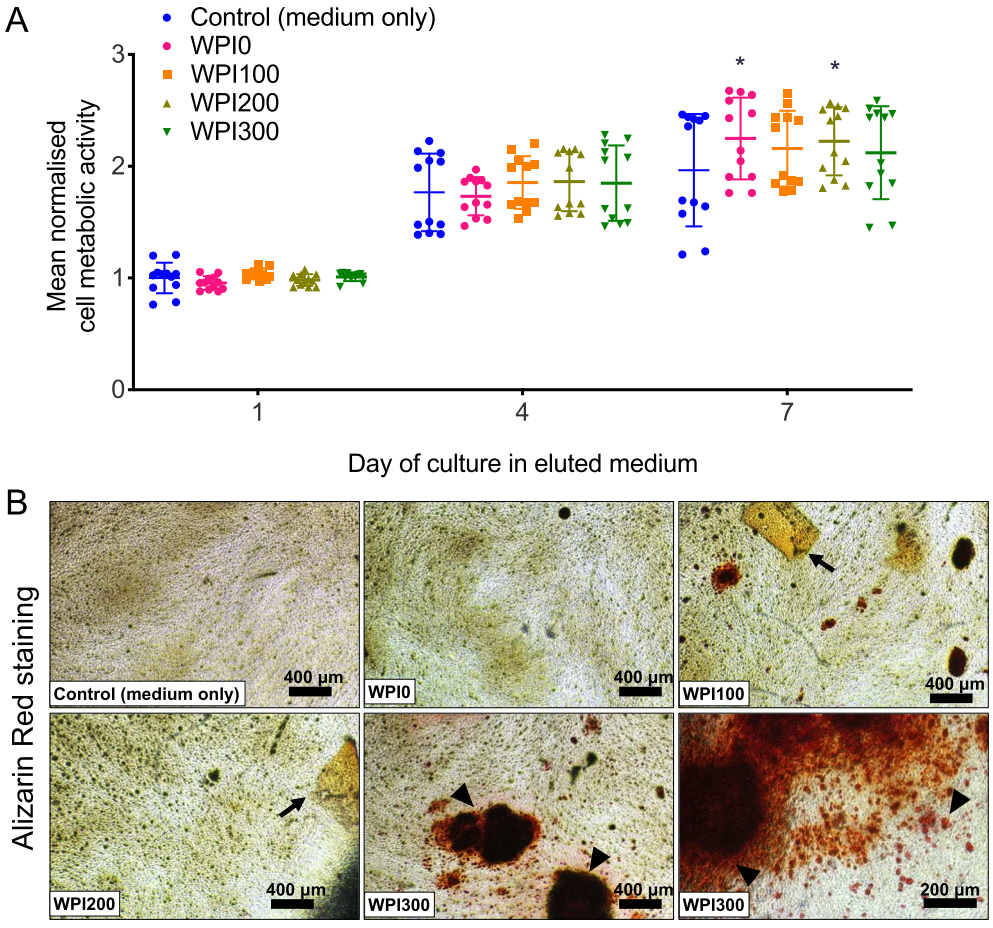

Fig. 6. Assessment of MG63 cytocompatibility with WPI-based biocomposites via indirect-contact experiments. (A) Mean ± S.D. of cell metabolic activity after over 7 days of culture in media conditioned with biocomposites ($n = 12$). * indicates $p < .05$, relative to control (medium only). (B) Alizarin Red stained cells after 21 days of exposure to conditioned media. Arrows - transparent debris, arrow heads - positive Alizarin red S staining. (For interpretation of the references to colour in this figure legend, the reader is referred to the web version of this article.)

study showed that WPI-aragonite biocomposites are cytocompatible and are potential candidates for bone tissue engineering applications. In future it would be interesting to investigate the response of bone marrow derived mesenchymal stem cells on WPI-based gels via assessment of gene expression and extracellular matrix deposition for bone regeneration applications.

5. Conclusion

The present work describes the physiochemical, mechanical, degradation and cytocompatibility properties of novel and inexpensive biocomposite hydrogels fabricated using WPI, a waste product of dairy industry and synthetic aragonite. The composites swelled more and released more protein under physiologically relevant degrading conditions as aragonite content increased from 0, 100, 200 to 300 mg/ml in the WPI solution. Mechanical strength also increased after addition of aragonite and the highest value was obtained for composites with 300 mg/ml of aragonite. All composites were porous pores >100 μm in diameter were present only in aragonite containing composites and the most even distribution of aragonite and pores was present in hydrogels with the highest aragonite content. The composites were supportive of osteoblast-like cell proliferation over a period of 3 weeks of culture and as the aragonite concentration increased, the cell proliferation and ALP activity was higher. The degradation products of these biocomposites were non-cytotoxic and may have induced mineralisation, indicating the osteoinductive nature of these biocomposites.

Funding

The micro-CT analyses were possible due to European Regional Development Fund through Competitiveness Operational Program 2014–2020, Priority axis 1, ID P_36_611, MySMIS code 107066, INOVABIOMED. TELD received the N8 AgriFood Pump-Priming grant “Food2Bone”.

Data availability

The authors declare that all the data related with this study are available within the paper or can be obtained from the authors on request.

CRediT authorship contribution statement

Dhanak Gupta: Data curation, Formal analysis, Investigation, Writing - original draft, Writing - review & editing, Supervision.**Magdalena Kocot:**Data curation, Writing - review & editing.**Anna Maria Tryba:** Data curation, Investigation, Writing - review & editing.**Andrada Serafim:**Data curation, Formal analysis, Writing - review & editing. **Izabela C. Stancu:**Data curation, Writing - review & editing.**Zbigniew Jaegermann:**Data curation, Writing - review & editing.**Elżbieta Pamuła:**Supervision, Resources, Writing - review & editing.**Gwendolen C. Reilly:**Supervision, Resources, Writing - review & editing.**Timothy E.L. Douglas:**Conceptualization, Supervision, Resources, Writing - review & editing.

Declaration of competing interest

The authors declare that they have no known competing financial interests or personal relationships that could have appeared to influence the work reported in this paper.

Appendix A. Supplementary data

Supplementary data to this article can be found online at https://doi.org/10.1016/j.matdes.2019.108408.

References

[1] E. Jimi, S. Hirata, K. Osawa, M. Terashita, C. Kitamura, H. Fukushima, The current and future therapies of bone regeneration to repair bone defects, Int J Dent 2012 (2012) 1–8.
[2] M.M. Stevens, Biomaterials for bone tissue engineering, Mater. Today 11 (5) (2008) 18–25.
[3] S. Patel, Emerging trends in nutraceutical applications of whey protein and its derivatives, J. Food Sci. Technol. 52 (11) (2015) 6847–6858.
[4] J.S.S. Yadav, S. Yan, S. Pilli, L. Kumar, R.D. Tyagi, R.Y. Surampalli, Cheese whey: a potential resource to transform into bioprotein, functional/nutritional proteins and bioactive peptides, Biotechnology Advances, 33, Elsevier Inc 2015, pp. 756–774.
[5] S. Ostojić, M. Pavlović, M. Živić, Z. Filipović, S. Gorjanović, S. Hranisavljević, et al., Processing of whey from dairy industry waste, Environ. Chem. Lett. 3 (1) (2005) 29–32.
[6] R.J.S. de Castro, M.A.F. Domingues, A. Ohara, P.K. Okuro, J.G. dos Santos, R.P. Brexó, et al., Whey protein as a key component in food systems: physicochemical properties, production technologies and applications, Food Struct. 14 (Oct) (2017) 17–29.
[7] R. Sharma, N. Shah, Health benefits of whey proteins, Nutrafoods 9 (4) (2010) 39–45.
[8] M.J. Spotti, Ö. Tarhan, S. Schaffter, C. Corvalan, O.H. Campanella, Whey protein gelation induced by enzymatic hydrolysis and heat treatment: comparison of creep and recovery behavior, Food Hydrocoll. 63 (2017) 696–704.
[9] G.E. Remondetto, E. Beyssac, M. Subirade, Iron availability from whey protein hydrogels: an in vitro study, J. Agric. Food Chem. 52 (26) (2004) 8137–8143.
[10] X. Bai, M. Gao, S. Syed, J. Zhuang, X. Xu, X.Q. Zhang, Bioactive hydrogels for bone regeneration, Bioact Mater 3 (4) (2018) 401–417.
[11] M. D'Este, D. Eglin, Hydrogels in calcium phosphate moldable and injectable bone substitutes: sticky excipients or advanced 3-D carriers? Acta Biomater. 9 (3) (2013) 5421–5430.
[12] M. Dziadek, R. Kudlackova, A. Zima, A. Slosarczyk, M. Ziabka, P. Jelen, et al., Novel multicomponent organic–inorganic WPI/gelatin/CaP hydrogel composites for bone tissue engineering, J Biomed Mater Res Part A (2019) 1–13.
[13] Y.C. Wu, T.M. Lee, K.H. Chiu, S.Y. Shaw, C.Y. Yang, A comparative study of the physical and mechanical properties of three natural corals based on the criteria for bone-tissue engineering scaffolds, J Mater Sci Mater Med 20 (6) (2009) 1273–1280.
[14] S.A. Clarke, P. Walsh, C.A. Maggs, F. Buchanan, Designs from the deep: marine organisms for bone tissue engineering, Aust. J. Dairy Technol. 29 (6) (2011) 610–617.
[15] R.T. Chiroff, E.W. White, J.N. Weber, D.M. Roy, Tissue ingrowth of replamineform implants, J. Biomed. Mater. Res. 9 (4) (1975) 29–45.
[16] L. Olah, K. Filipczak, Z. Jaegermann, T. Czigany, L. Borbas, S. Sosnowski, et al., Synthesis, structural and mechanical properties of porous polymeric scaffolds for bone tissue regeneration based on neat poly(e-caprolactone) and its composites with calcium carbonate, Polym. Adv. Technol. 12 (2006) 889–897.
[17] V. Viateau, M. Manassero, L. Sensébé, A. Langonné, D. Marchat, D. Logeart-Avramoglou, et al., Comparative study of the osteogenic ability of four different ceramic constructs in an ectopic large animal model, J. Tissue Eng. Regen. Med. 10 (3) (2010) E177–E187.
[18] M. Doube, M.M. Klosowski, I. Arganda-Carreras, F.P. Cordelières, R.P. Dougherty, J.S. Jackson, et al., BoneJ: free and extensible bone image analysis in ImageJ, Bone 47 (6) (2010) 1076–1079.
[19] A. Shafiu Kamba, M. Ismail, T.A. Tengku Ibrahim, Z.A.B. Zakaria, Synthesis and characterisation of calcium carbonate aragonite nanocrystals from cockle shell powder (Anadara granosa), J. Nanomater. 5 (2013).
[20] M. Toffolo, L. Regev, S. Dubernet, Y. Lefrais, E. Boaretto, FTIR-based crystallinity assessment of aragonite–calcite mixtures in archaeological lime binders altered by diagenesis, Minerals 9 (2) (2019) 121.
[21] B.D. Valtierra, FTIR Investigations of Whey Protein Interactions in Relation to Model Food Systems, McGill University, 2015.
[22] N. Datta, H.C. Deeth, High pressure processing of milk and milk products, N Datta ; H C Deeth Aust. J. Dairy Technol. 54 (1999) 41–48.
[23] A.L. Gillespie, D. Calderwood, L. Hobson, B.D. Green, Whey proteins have beneficial effects on intestinal enteroendocrine cells stimulating cell growth and increasing the production and secretion of incretin hormones, Food Chem. 189 (2015) 120–128.
[24] Y. Takada, S. Aoe, M. Kumegawa, Whey protein stimulated the proliferation and differentiation of osteoblastic MC3T3-E1 cells, Biochem. Biophys. Res. Commun. 223 (2) (1996) 445–449.
[25] R. Xu, Effect of whey protein on the proliferation and differentiation of osteoblasts, J. Dairy Sci. 92 (7) (2009) 3014–3018.
[26] T.E.L. Douglas, M. Vandrovcová, N. Kročilová, J.K. Keppler, J. Zárubová, A.G. Skirtach, et al., Application of whey protein isolate in bone regeneration: effects on growth and osteogenic differentiation of bone-forming cells, J. Dairy Sci. 101 (1) (2018) 28–36.
[27] M. Carson, J.K. Keppler, G. Brackman, D. Dawood, M. Vandrovcova, K. Fawzy El-Sayed, et al., Whey protein complexes with green tea polyphenols: antimicrobial, osteoblast-stimulatory, and antioxidant activities, Cells Tissues Organs 206 (1–2) (2018) 106–117.
[28] C.S. Tai, Y.Y. Chen, W.L. Chen, β-Lactoglobulin influences human immunity and promotes cell proliferation, Biomed. Res. Int. 2016 (2016).
[29] V. Karageorgiou, D. Kaplan, Porosity of 3D biomaterial scaffolds and osteogenesis, Biomaterials 26 (27) (2005) 5474–5491.
[30] Z. A a, Bone tissue regeneration: the role of scaffold geometry, Biomater Sci 3 (2) (2015) 231–245.
[31] B. Habel, R. Glaser, Human osteoblast-like cells respond not only to the extracellular calcium concentration but also to its changing rate, Eur. Biophys. J. 27 (4) (1998) 411–416.

[32] S. Maeno, Y. Niki, H. Matsumoto, H. Morioka, T. Yatabe, A. Funayama, et al., The effect of calcium ion concentration on osteoblast viability, proliferation and differentiation in monolayer and 3D culture, Biomaterials 26 (23) (2005) 4847–4855.
[33] P. Juin, M. Pelletier, L. Oliver, K. Tremblais, M. Grégoire, K. Meflah, et al., Induction of a caspase-3-like activity by calcium in normal cytosolic extracts triggers nuclear apoptosis in a cell-free system, J. Biol. Chem. 273 (28) (1998) 17559–17564.
[34] S. Radin, G. Reilly, G. Bhargave, P.S. Leboy, P. Ducheyne, Osteogenic effects of bioactive glass on bone marrow stromal cells, J Biomed Mater Res - Part A 73 (1) (2005) 21–29.
[35] J. Yao, S. Radin, G. Reilly, P.S. Leboy, P. Ducheyne, Solution-mediated effect of bioactive glass in poly (lactic-co-glycolic acid)-bioactive glass composites on osteogenesis of marrow stromal cells, J Biomed Mater Res - Part A 75 (4) (2005) 794–801.